Nano-Structures & Nano-Objects 20 (2019) 100388

Contents lists available at ScienceDirect

Nano-Structures & Nano-Objects

journal homepage: www.elsevier.com/locate/nanoso

Effect of Nd-doping on soot oxidation activity of Ceria-based nanoparticles synthesized by Glycine Nitrate Process

Sunaina S Patil [a], Hari Prasad Dasari [a,*], Harshini Dasari [b]

[a] Chemical Engineering Department, National Institute of Technology Karnataka, Surathkal, Mangalore 575025, Karnataka, India
[b] Chemical Engineering Department, Manipal Institute of Technology, Manipal Academy of Higher Education (MAHE) Manipal, Udupi 576104, Karnataka, India

ARTICLE INFO

Article history:
Received 24 April 2019
Received in revised form 29 July 2019
Accepted 27 August 2019

Keywords:
Neodymium-doped Ceria
XPS analysis
Redox potential
Surface active oxygen species
Soot oxidation

ABSTRACT

Neodymium-doped Ceria (NDC, Nd = 0, 1, 3, 5, 10, 20 and 30 mol %) catalysts were successfully synthesized by Glycine-Nitrate-Process (GNP) and tested for soot oxidation activity. For all NDC catalysts, XRD and Raman spectroscopy analyses showed a fluorite structure of ceria having an F_{2g} Raman active symmetric breathing mode (O-Ce-O). 1NDC catalyst displayed better T_{50} temperature (427°C) followed by 0NDC (435°C), and 30NDC showed the highest T_{50} temperature (460°C). From XPS analysis, 1NDC and 0NDC catalysts showed a high amount of Ce^{3+} concentration and the surface-active oxygen species than compared to other NDC catalysts and thus, resulted in better soot oxidation activity indicating that the surface Ce^{3+} concentration and surface-active oxygen species play a key descriptor role in tuning the soot oxidation activity of NDC catalysts.

1. Introduction

Soot is an impure particulate matter of diesel/ fuel produced due to partial combustion of hydrocarbons. It is harmful to human lungs and also deteriorates the exhaust system of vehicles [1]. Hence, recognizing promising catalysts capable of replacing the existing costly catalysts to assist soot oxidation is essential. Developing catalysts for soot oxidation may primarily involve discovering the materials, which have excellent Oxygen Storage Capacity (OSC), high surface area, and other parameters, which can enhance the catalytic activity. Grasselli [2] described the key descriptors, which may play a vital role in selective oxidation catalysis to understand the catalyst behavior. It has been reported that seven principles or pillars for oxidation catalysis comprises the availability of lattice oxygen, desired metal-oxygen bond strength in appropriate host structure, co-operation of the phases, redox properties of active sites, site-isolation, lattice oxygen and multi-functionality [2,3]. For ceria-based materials, fixation of a single descriptor is not possible, and multiple descriptors control the activity depending on the various reaction conditions.

Rare earth elements like Ceria (CeO_2), which exhibits both the 3+ and 4+ oxidation states have attained significance over the past few decades due to its unique properties and applications. CeO_2 based materials subsequently induce high OSC [4,5]. Doping of trivalent lanthanides in cubic structured CeO_2 is a favorable technique which develops Oxygen (O_2) vacancies at the octahedral sites and creates defects which alter the diffusive performance and thus gains interest in the area of research [5]. CeO_2 catalysts also encourage diesel particulate filter regeneration by reducing the required temperature to oxidize soot. In the recent development, CeO_2-based catalysts have improved the contact between catalyst and soot [6–8].

Researches have evaluated performance of transition metal oxides and oxides of lanthanides namely CeO_2 [9–11], Zirconium (Zr), Manganese (Mn), Praseodymium (Pr), Hafnium (Hf), Lanthanum (La), Samarium (Sm), Tin (Sn), and Gadolinium (Gd) for soot oxidation. According to Anantharaman et al. [9], the T_{50}temperature for single oxide materials reported in the range of 482∼530 °C. Lower T_{50}temperature (445 °C–396 °C) was obtained for nanostructured CeO_2, as nano-shaped catalysts play a critical role by affecting the active sites and oxygen defect formation which helps in enhancing the catalytic activity [12,13]. Soot oxidation activity over CeO_2-based catalysts (Ce–Pr [8,14,15], Ce–Zr [10,11,16], Ce–La [10], Ce–Mn [8,17,18], Ce–Sm [6] and Ce–Gd [7,19]) were also reported in the literature. T_{50} temperature for CeO_2-based materials is in the range of 533–409 ° C [6–26]. Vazquez et al. [27] reported more efficient soot combustion in the presence of 1 wt % Mn-doped $SrTiO_3$.

In the present study, Neodymium (Nd) is selected as a dopant due to its higher solubility in CeO_2 and higher O_2 diffusion coefficient compared to many other rare earth materials [1]. NDC is believed to have enhanced catalytic activity in most of the applications and has already gained popularity in the field of

* Correspondence to: Chemical Engineering Department, National Institute of Technology Karnataka, Mangalore 575025, India.
E-mail address: energyhari@nitk.edu.in (H.P. Dasari).

https://doi.org/10.1016/j.nanoso.2019.100388
2352-507X/

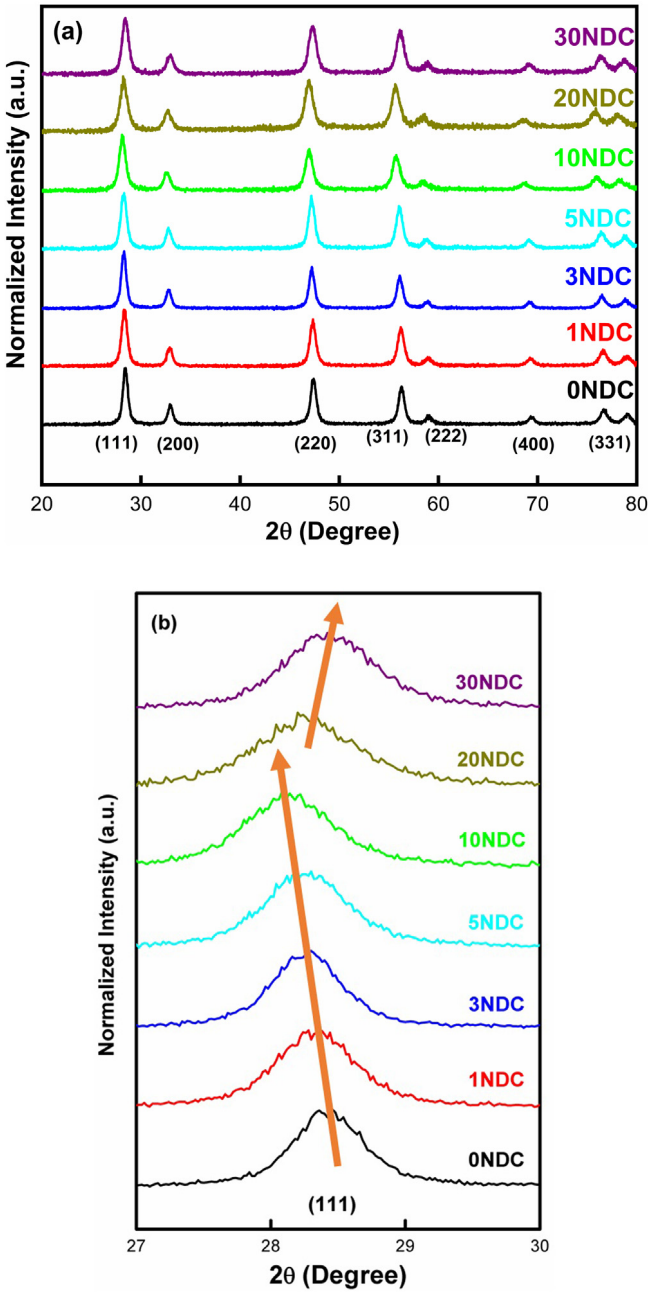

Fig. 1. (a) XRD patterns and (b) Enlarged view of the (111) plane from XRD patterns of NDC catalysts synthesized by GNP calcined at 600 °C/2 h.

electrolytes and Solid oxide fuel cells (SOFC) [28–31]. Few examples were reported for Nd-doped Ce–Zr catalysts or Nd-doped as co-dopant to Ce based materials for soot oxidation. It was also reported that Nd improved the catalytic activity for binary Ce based materials [32–34].

Synthesis method also plays a vital role in developing uniform and stable nanoparticles. Researches also reported the synthesis of Nano-catalysts through Solution Combustion Synthesis (SCS) [35,36] method using Glycine Nitrate Process (GNP) [37–43], Sol–gel method [18,33,44], co-precipitation method reverse co-precipitation-calcination method [44,45], EDTA citrate method [9] etc. GNP is found to be the most effective method as it produces fine, homogeneous particles is relatively less costly and also has higher energy efficiency [37,38]. Apart from the advantages mentioned above, this method also has fast heating rates and short reaction time [39]. Generally, in the SCS or GNP, the formation of the precursor solution is followed by Auto-Ignition Process (AIP) where the heat of combustion is generated, and gases are evolved [37,38]. To control the combustion reaction in this process, the fuel-rich precursor is used, which also results in giving the phase pure composition [37,38,40,46]. The ratio of Glycine/Nitrate (G/N) is a vital processing variable, which plays a crucial role in controlling the combustion flame temperature, the combustion velocity, and the product morphology.

In the present paper, we report the synthesis of NDC catalysts (0NDC–30NDC) with Nd concentration varying as 0, 1, 3, 5, 10, 20 and 30 mol% via GNP by employing fuel-rich condition where Glycine serves as a fuel in GNP for combustion. Glycine gets oxidized by the nitrate ions and also helps in avoiding selective precipitation in the precursor solution by complexing with the metal cations [39]. Furthermore, the synthesis of nanoparticles using GNP lead to the production of particles with lesser crystallite size as compared to synthesis using other fuels [36,43]. The synthesized NDC catalysts were characterized and tested for soot oxidation activity.

2. Experimental details

2.1. Catalyst preparation

NDC samples (Nd = 0∼30 mol %) were successfully synthesized by GNP. The stoichiometric amount of Nitrates [$(Ce(NO_3)_3 \cdot 6H_2O$ and $Nd(NO_3)_3 \cdot 6H_2O$)] and glycine were mixed in distilled water. The ratio of Glycine/Nitrate ratio was fixed at 0.35 [47]. Both nitrates and fuel readily dissolved in distilled water. The obtained solution was heated and stirred continuously at 70 °C, which then turned into a transparent viscous gel. Subsequently, the gel was transferred into a pre-heated oven at 250 °C where it auto-ignited to give combustion powder product, which was further calcined at 600 °C for 2 h in the air to get the final catalyst powder.

2.2. Catalyst characterization

The obtained nanopowder was characterized using X-ray Diffraction (XRD — Rigaku Miniflex 600), FT-Raman spectroscopy (BRUKER RFS27) with 785 nm laser beam, surface area analyzer (SMART SORB-92/93), SEM (SEM- JEOL/JSM 6390LV) and TEM (TEM-JEOL/JEM 2100) instruments. The multiple oxidation states and the oxygen vacancies of the NDC samples were analyzed using the X-ray Photon Spectroscopy (XPS) (Omicron ESCA+) in an ultrahigh vacuum. The base pressure during the XPS analysis was 5×10^{-9} torr operated at a power of 300 watts using Al K α mono source. The peaks were deconvoluted, and the data was analyzed using Casa-XPS Software (Version No. 2.3.19 PR 1.0). The spectra were calibrated to the standard binding energy (B.E) value of 284.6 eV of carbon 1s. Photoluminescence Spectra (PLS) were recorded in [Horiba Fluoromax 4] Spectrofluorometer (excitation wavelength of 320 nm). Ultraviolet Visible Diffusive Reflectance and Absorption Spectra (UV-Vis DRS) of the samples were obtained in (Varian Cary 5000) UV Spectrophotometer.

2.3. Soot oxidation activity

Catalytic activity was performed with soot: catalyst ratio of 1:10 under tight contact condition. The soot (Printex U (Orion Engineered Carbons)) and catalyst (NDC samples) mixture were ground using mortar and pestle for 30 min to ensure proper tight contact condition. TGA (TG/DTA 6300 (Hitachi)) instrument was used to carry out soot oxidation activity in the air at a flow rate of 100ml/min with a heating rate of 10 °C/min from room temperature to 600 °C. The reproducibility of the catalytic activity was obtained for all the samples.

Table 1
Crystallite size (D_{XRD}), lattice strain (ϵ), BET surface area (S_A), particle size from BET (D_{BET}), degree of agglomeration (Φ) and optical band gap value (eV) of NDC catalysts.

Sample	Crystallite size D_{XRD} (nm)	Lattice strain (ε)	BET surface area S_A (m^2/g)	Particle size from BET analysis D_{BET} (nm)	Φ (D_{XRD}/D_{BET})	Optical band gap value (eV)
0NDC	14	0.0104	19	43	0.326	3.01
1NDC	12	0.0122	23	36	0.330	2.99
3NDC	14	0.0105	32	26	0.545	2.98
5NDC	12	0.0128	21	39	0.292	2.97
10NDC	11	0.0137	15	57	0.190	2.91
20NDC	09	0.0161	27	31	0.297	2.87
30NDC	11	0.0139	18	47	0.225	2.86

3. Results and discussion

3.1. XRD analysis

Fig. 1a depicts the XRD patterns of NDC catalysts (Nd = 0 to 30 mol %) synthesized by GNP and calcined at 600 °C/2 h in air. XRD patterns of all the NDC catalysts exhibit similar peaks corresponding to the planes of a fluorite structure of CeO_2 [9,39]. Peaks corresponding to Nd_2O_3 were not observed, indicating that the Nd was completely soluble in CeO_2 lattice and formed an NDC solid solution [48]. A slight shift of (111) peak towards lower 2θ value for NDC samples (Nd = 0 to 10 mol%) was observed and this may be due to replacement of smaller ionic radius (Ce^{4+} = 1.01 Å) with larger ionic radius (Nd^{3+} = 1.12 Å) [49,50]. With further increase in Nd mol% in the NDC samples (Nd = 20 and 30 mol %) the (111) peak shifted towards higher 2θ values indicating the saturation of Nd in NDC solid solution as observed in Fig. 1b. From the XRD data, the crystallite size (D_{XRD}), lattice strain (ε) of NDC catalysts were calculated and tabulated in Table 1 along with the BET surface area (S_A), particle size obtained from the BET surface area (D_{BET}) and degree of agglomeration (Φ). Crystallite size obtained for the synthesized samples was in the range of 9–14 nm. Lattice Strain was the lowest for 0NDC sample (0.0104) and the highest for 20NDC sample (0.0161). BET specific surface area (S_A) was found to be lowest (14 m^2/g) for a 10NDC sample and the highest (32 m^2/g) for 3NDC sample. The particle size obtained from BET surface area was in the range of 26 nm to 57 nm, and the degree of agglomeration was lowest for 3NDC sample compared to all other NDC catalysts.

3.2. UV-Vis DRS analysis

The UV spectra for the NDC catalysts are provided in Fig. 2a, and it can be seen that for the 0NDC sample, the bands at 255, 274 and 338 nm correspond to the pure CeO_2 charge transfer and inter-band transitions [4,51]. All the NDC catalysts displayed similar bands at 255, 274 and 338 nm, indicating that there is not much change in the band position which thereby confirmed that there is no change in the Ce^{3+}/Ce^{4+} fraction on the surface of NDC catalysts [4,51]. For 5NDC–30NDC samples, it is interesting to observe that additional bands located in between 500∼750 nm and these other bands correspond to the presence of Nd in the NDC sample. For 1NDC and 3NDC samples, these other peaks were not observed, indicating that 1 and 3 mol% of Nd^{3+}ions may not be well settled in CeO_2 lattice [51]. Since the other bands related to Nd were noticed at 525, 590 and 747 nm in the UV–Vis DRS spectra, for Raman analysis, a higher wavelength of 785 nm had been adopted so that complete bulk information of the NDC samples can be obtained.

From the information obtained from UV–Vis spectra (Fig. 2a), a Tauc's plot was generated for all the NDC samples and depicted in Fig. 2b. From the Tauc's plot, the optical band gap value of each NDC sample was calculated and is shown in Table 2. The optical band gap energy value of all the samples was in the range of 2.80 to 3.10 eV. 0NDC and 30 NDC displayed highest (3.01 eV) and lowest (2.86 eV) optical band gap values respectively. It can also be noticed that, with the increase in Nd concentration in CeO_2, the optical band gap value had reduced.

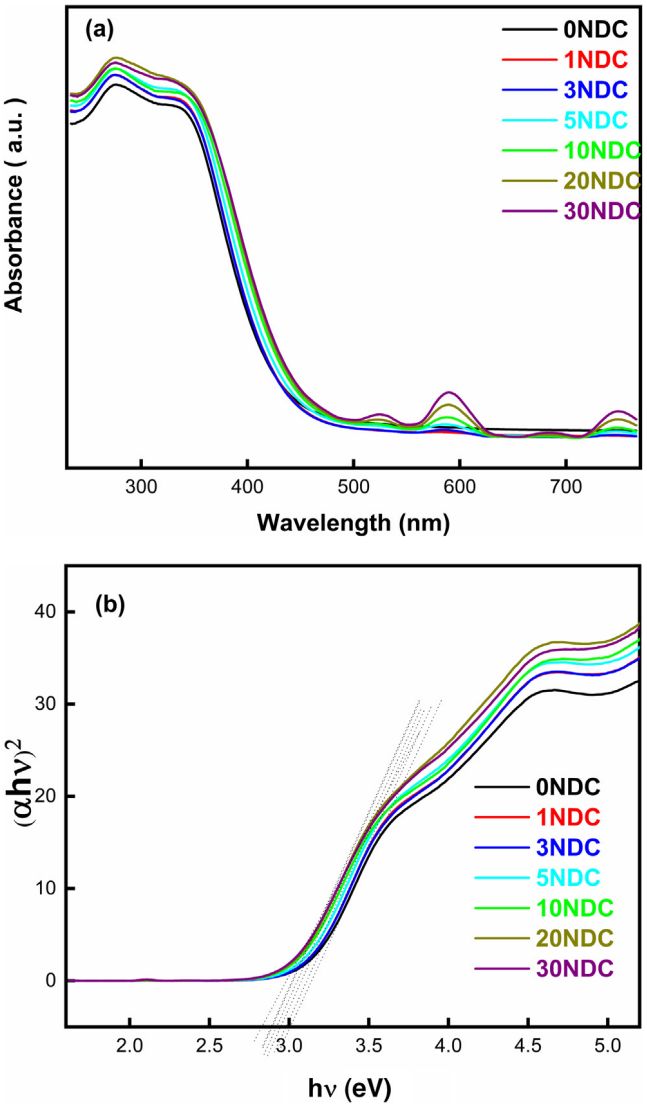

Fig. 2. (a) UV–Vis DR spectra and (b) Tauc's plot to determine the optical band gap of NDC catalysts synthesized by GNP calcined at 600 °C/2 h.

3.3. Raman spectroscopy analysis

The Raman spectra of the NDC samples are depicted in Fig. 3. The Raman frequency at 462 cm^{-1} confirmed the formation of NDC solid-solution prepared by GNP. The distinct band at

Table 2
Reducibility ratio, the ratio of Surface Oxygen species and T_{50} Temperatures of NDC catalysts.

Sample	Reducibility ratio (%)	Surface Oxygen species (%)			T_{50} (°C)
		Lattice Oxygen	Adsorbed Oxygen		
	$\frac{Ce^{3+}}{(Ce^{3+}+Ce^{4+})}$	$\frac{O^{2-}}{(O^{2-}+O^{-}+O_2^{-})}$	$\frac{O^{-}}{(O^{2-}+O^{-}+O_2^{-})}$	$\frac{O_2^{-}}{(O^{2-}+O^{-}+O_2^{-})}$	
0NDC	33	64	33	3	435
1NDC	48	48	45	7	427
3NDC	33	67	18	15	440
5NDC	28	67	16	17	450
10NDC	43	65	27	8	456
20NDC	27	43	35	22	460
30NDC	36	47	43	9	461

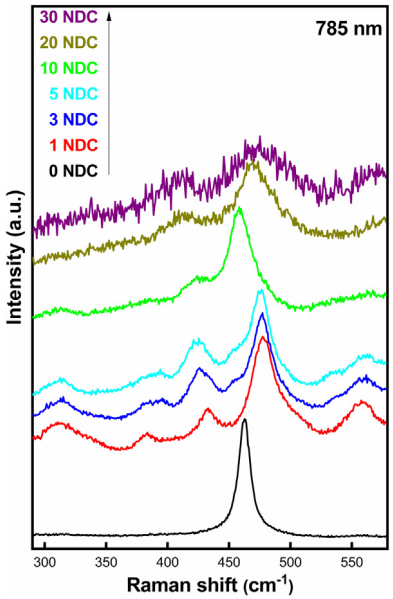

Fig. 3. Raman spectra of NDC catalysts synthesized by GNP calcined at 600 °C/2 h.

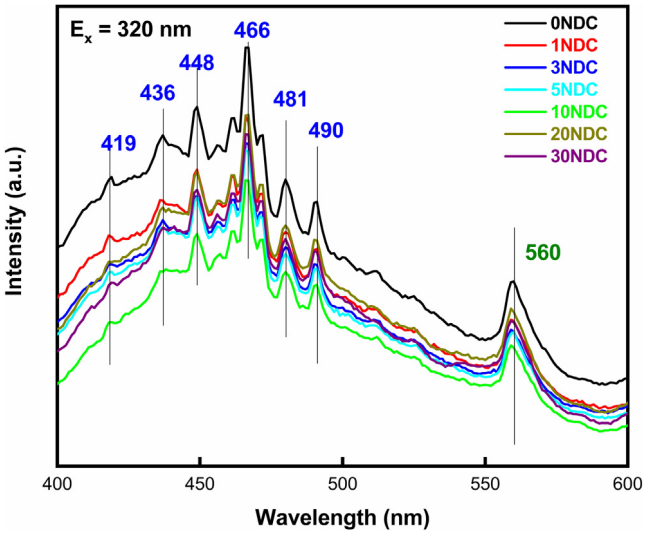

Fig. 4. Photoluminescence curves of NDC catalysts synthesized by GNP calcined at 600 °C/2 h.

462 cm^{-1} can be associated to the F_{2g} Raman mode (O–Ce–O) [9,17]. Compared to 0NDC sample, there was a slight shift in F_{2g} peak position of doped samples towards higher wavenumber and was due to changes in metal-oxygen coordination [52]. The weak band at 560 cm^{-1} could be due to the presence of the oxygen vacancies created in CeO_2 to maintain the charge neutrality [53]. The other peaks at 310, 382, 430 cm^{-1} may correspond to the secondary degenerate of the weak band at 560 cm^{-1}. Apart from that, no additional peaks related to Nd_2O_3 were detected in the spectra [52].

3.4. Photoluminescence (PL) studies

Fig. 4 illustrates the PL spectra of NDC samples. The PL intensity of doped samples decreased, and this may be attributed to the release of excess energy by the transition of electrons from Ce 4f to O 2p orbitals [54]. The emission peaks observed in the spectral range of 425 to 680 nm are related to O_2 vacancies [51,54,55]. There was no evidence of Nd associated peaks in the obtained PL spectra, and no changes in the peak positions were observed. It can be concluded that Nd doping increases the O_2 vacancy concentration corroborating with the results obtained from Raman spectra, and thus, this factor may also affect the catalytic activity [52].

3.5. TEM analysis

Fig. 5a shows the TEM images of the NDC samples (Nd = 0, 1, 5, 20 mol %). Fig. 5a confirms that the samples prepared are of nano-scale in the range of 8∼23 nm. The obtained nanoparticles were agglomerated and were almost spherical. The inter-planer distance was measured and calculated from the lattice fringes in the HR-TEM image (Fig. 5b) with the insight of SAED patterns, which confirmed that the synthesized samples were polycrystalline. The values obtained from HR-TEM correspond to the planes of fluorite structure of CeO_2, which are in good agreement with XRD analysis.

3.6. Soot oxidation activity

Fig. 6 demonstrates the soot oxidation activity of the NDC catalysts and the corresponding T_{50} temperatures are given in Table 2. The catalytic activity with respect to T_{50} temperatures of the NDC catalysts is as follows; 1NDC > 0NDC > 3NDC > 5NDC > 10NDC > 20NDC > 30NDC. The obtained results show that 1NDC and 0NDC catalysts displayed better soot oxidation activity than the other NDC samples, and the activity decreased with the increase of Nd from 3 to 30 mol%. Figs. S2a, and S2b shows the reproducibility of the soot oxidation activity of 1NDC and 0NDC catalysts and reconfirms activity. Similar results were reported in the literature [27,56] in which 1 wt % or 1 mol% addition of the dopant enhanced the catalytic activity. Vazquez et al. [27] reported that 1 wt % Mn-doped $SrTiO_3$ displayed better

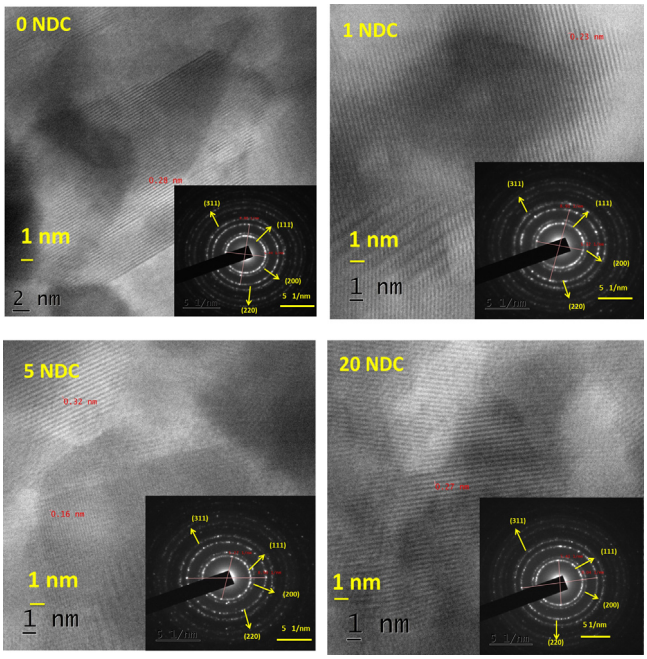

Fig. 5. (a)TEM and (b) HR-TEM micrographs with corresponding selected-area electron diffraction (SAED) patterns of NDC catalysts (0,.1, 5, 20 mol %) synthesized by GNP calcined at 600 °C/2 h.

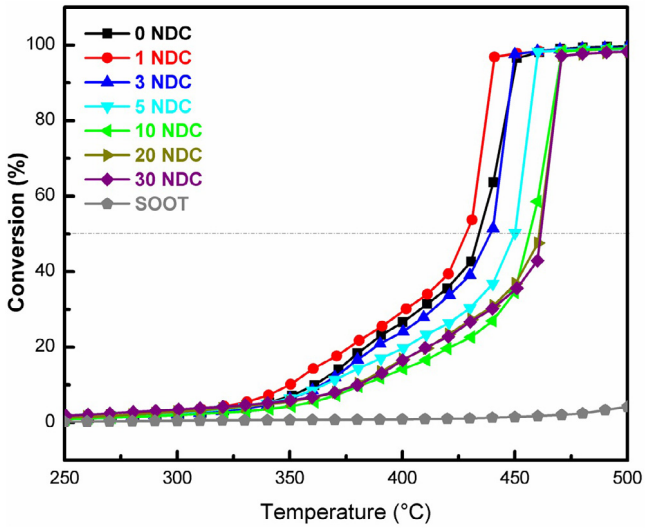

Fig. 6. Soot conversion (%) versus reaction temperature (°C) of Soot and NDC catalysts synthesized by GNP calcined at 600 °C/2 h.

catalytic activity for soot oxidation activity due to lower activation energy and enhanced mobility of the bulk O_2 to the surface. Pengpanich et al. [56] reported that 1 wt% Nb-doped in Ce–Zr enhanced that catalytic activity for methane oxidation due to high reducibility (Ce^{3+} / (Ce^{3+} + Ce^{4+})) of CeO_2. Andrew Getsoian et al. [57] showed the bandgap energy as a descriptor for propene oxidation activity over mixed metal oxide catalysts. Grasselli et al. [2], postulated the principle seven descriptors (redox, phase cooperation, host structure, lattice oxygen, metal-oxygen bond, multi-functionality of the active sites and site isolation) to define the activity for oxidation reactions and it is difficult to map to a specific descriptor as a key player directly.

3.7. XPS analysis

Surface analysis of the NDC catalysts was carried out and is depicted in Fig. 7a. The corresponding eight peaks related to Ce^{3+} and Ce^{4+}oxidation states were analyzed [58,59]. From XPS analysis, as shown in Table 2, the relative amount of Ce^{3+} concentration (Ce^{3+}/(Ce^{3+} + Ce^{4+})) is high for 1NDC catalyst as compared to other NDC catalysts indicating a higher concentration of surface oxygen vacancies [60]. Fig. 7b depicts the O1s spectra of NDC samples. The O1s spectra provide the information of the three different O_2 species corresponding to the lattice oxygen species (O^{2-}) and the chemisorbed oxygen species (O^- and O_2^-) located at 529, 530 and 532 eV, respectively [61]. From Table 2, the highest surface-active O_2 species ratio [O^-/(O^{2-} + O^- + O_2^-)] is obtained for 1NDC catalysts than the other NDC catalysts, which agrees well with the Ce 3d spectra results. It can be inferred that the Nd^{3+} doping favors the formation of surface-active O_2 species (O^-) only for 1NDC and further addition of Nd^{3+} decreased the amount of surface-active O_2 species (O^-) which is confirmed from XPS analysis. High surface active oxygen species ratio favors 1NDC catalyst to have better soot oxidation activity than compared to other NDC catalysts and is consistent with the literature where the surface active oxygen species (O^-) is essential for low temperatures soot oxidation activity [61]. As the temperature increases, both surface-active O_2 species (O^-) and lattice O_2 species (O^{2-}) promote the soot oxidation activity [61]. From the XPS analysis and soot oxidation activity results of NDC catalysts, 1NDC and 0NDC showed higher amounts of surface-active O_2 species (O^-) and displayed better soot oxidation activity at low temperatures. The current study also suggests that the type and dopant concentration in CeO_2 plays an essential role in fine-tuning of the redox potential and surface-active O_2 species (O^-) that can affect the activity at low temperatures and can act as a key descriptor.

4. Conclusion

Using Glycine-Nitrate-Process (GNP), Neodymium doped Ceria (NDC) catalyst nanoparticles were successfully synthesized and tested for soot oxidation activity. It was found that the Nd doping affects the physicochemical properties of the NDC catalysts. XRD and Raman spectroscopy provided evidence of phase cooperation (no secondary phase of Nd was noticed in the NDC samples). TEM analysis revealed a similar surface morphology and the particle size was in the range of 6∼15 nm for the NDC catalysts. The soot oxidation activity enhancement for 1NDC and 0NDC catalysts could be related to the enhancement of redox potential and surface-active O_2 (O^-) species (as detected by XPS technique). The type and dopant concentration in CeO_2 play an important role in fine-tuning of the redox potential and surface-active O_2 species (O^-) that can affect the soot oxidation activity at low temperatures and can act as a key descriptor.

Declaration of competing interest

The authors declare that they have no known competing financial interests or personal relationships that could have appeared to influence the work reported in this paper.

Acknowledgments

The present work is funded by DST SERB (ECR/2016/002010) and partially funded by DST SERB (EMR/2016/002592). SP is grateful to NITK for allowing carrying out the research work and to HPD for guidance. We would like to express our gratitude towards the Department of Physics, NITK for providing PLS data and Department of Metallurgical & Materials Engineering, NITK for SEM analysis. We would like to thank SAIF STIC, Cochin for facilitating TEM and UV–Vis/DRS data. We also acknowledge MRC, MNIT Jaipur for providing XPS and FT Raman data.

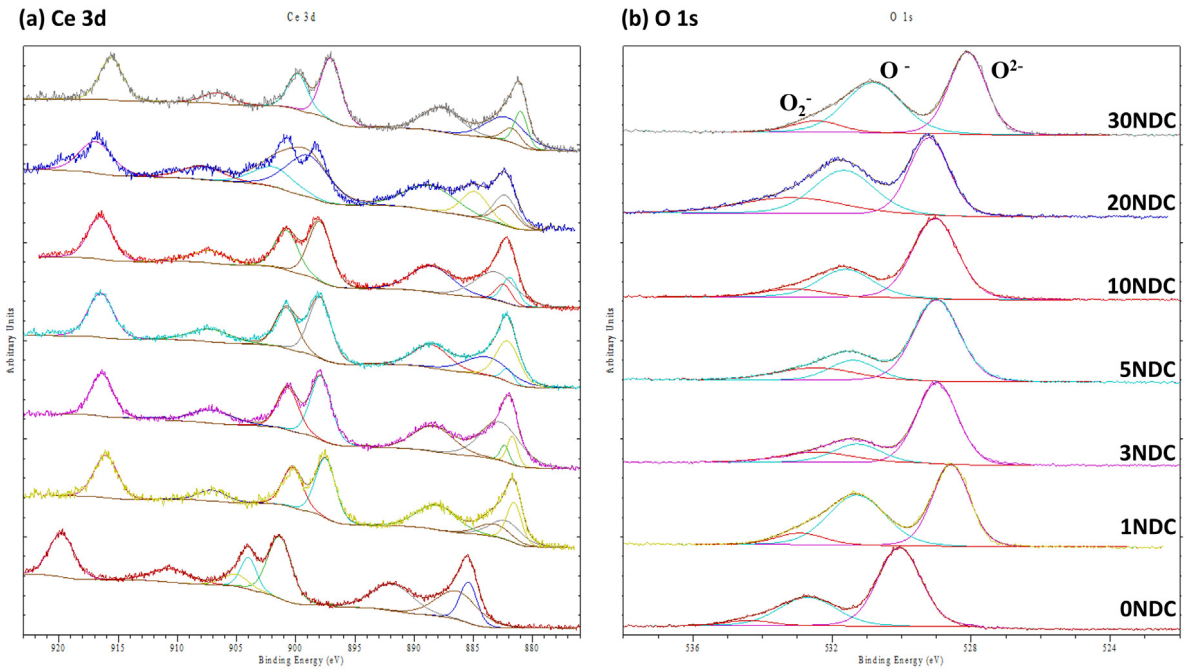

Fig. 7. (a) Ce 3d XP spectra and (b) O 1s XP spectra of NDC catalysts synthesized by GNP calcined at 600 °C/2 h.

Appendix A. Supplementary data

Supplementary material related to this article can be found online at https://doi.org/10.1016/j.nanoso.2019.100388.

References

[1] H. Omidvarborna, A. Kumar, D.S. Kim, Recent studies on soot modeling for diesel combustion, Renew. Sustain. Energy Rev. 48 (2015) 635–647, http://dx.doi.org/10.1016/j.rser.2015.04.019.

[2] R.K. Grasselli, Fundamental principles of selective heterogeneous oxidation catalysis, 21 (2002) 79–88.

[3] G. Vilé, D. Teschner, J. Pérez-ramírez, N. López, Appl. Catal. B 197 (2016) 299–312, http://dx.doi.org/10.1016/j.apcatb.2016.02.035.

[4] D.H. Prasad, S.Y. Park, H.-I. Ji, H.-R. Kim, J.-W. Son, B.-K. Kim, H.-W. Lee, J.-H. Lee, Structural characterization and catalytic activity of $Ce_{0.65}$ $Zr_{0.25}$ RE $_{0.1}$ $O_{2-\delta}$ nanocrystalline powders synthesized by the glycine-nitrate process, J. Phys. Chem. C 116 (2012) 3467–3476, http://dx.doi.org/10.1021/jp207107j.

[5] M. Jamshidijam, R.V. Mangalaraja, A. Akbari-Fakhrabadi, S. Ananthakumar, S.H. Chan, Effect of rare earth dopants on structural characteristics of nanoceria synthesized by combustion method, Powder Technol. 253 (2014) 304–310, http://dx.doi.org/10.1016/j.powtec.2013.10.032.

[6] P. Sudarsanam, K. Kuntaiah, B.M. Reddy, Promising Ceria-samaria-based nano-oxides for low temperature soot oxidation: A combined study of structure–activity properties, New J. Chem. 38 (2014) 5991–6001, http://dx.doi.org/10.1039/c4nj01274g.

[7] D.N. Durgasri, T. Vinodkumar, F. Lin, I. Alxneit, B.M. Reddy, Gadolinium doped cerium oxide for soot oxidation: Influence of interfacial metal-support interactions, Appl. Surf. Sci. 314 (2014) 592–598, http://dx.doi.org/10.1016/j.apsusc.2014.07.036.

[8] D. Mukherjee, B.G. Rao, B.M. Reddy, CO and soot oxidation activity of doped Ceria: Influence of dopants, Appl. Catal. B 197 (2016) 105–115, http://dx.doi.org/10.1016/j.apcatb.2016.03.042.

[9] Anjana P. Anantharaman, Hari Prasad Dasari, Jong-Ho Lee, G.U.B. Babu, Harshini Dasari, Soot oxidation activity of redox and non-redox metal oxides synthesised by EDTA-citrate method, Catal. Lett. 147 (2017) 1–13.

[10] L. Katta, P. Sudarsanam, G. Thrimurthulu, B.M. Reddy, Doped nanosized Ceria solid solutions for low temperature soot oxidation: Zirconium versus lanthanum promoters, Appl. Catal. B 101 (2010) 101–108, http://dx.doi.org/10.1016/j.apcatb.2010.09.012.

[11] B.M. Reddy, P. Bharali, G. Thrimurthulu, P. Saikia, L. Katta, S.E. Park, Catalytic efficiency of Ceria-zirconia and Ceria-hafnia nanocomposite oxides for soot oxidation, Catal. Lett. 123 (2008) 327–333, http://dx.doi.org/10.1007/s10562-008-9427-3.

[12] W. Zhang, X. Niu, L. Chen, F. Yuan, Y. Zhu, Soot combustion over nanostructured Ceria with different morphologies, Nat. Publ. Gr. 6 (2016) 29062, http://dx.doi.org/10.1038/srep29062.

[13] E. Aneggi, D. Wiater, C. De Leitenburg, J. Llorca, A. Trovarelli, Shape-dependent activity of Ceria in soot combustion, ACS Catal. 4 (2014) 172–181, http://dx.doi.org/10.1021/cs400850r.

[14] K. Krishna, A. Bueno-López, M. Makkee, J.A. Moulijn, Potential rare-earth modified CeO_2 catalysts for soot oxidation. Part III. Effect of dopant loading and calcination temperature on catalytic activity with O_2 and NO + O_2, Appl. Catal. B 75 (2007) 210–220, http://dx.doi.org/10.1016/j.apcatb.2007.04.009.

[15] T. Andana, M. Piumetti, S. Bensaid, N. Russo, D. Fino, Nanostructured Ceria-praseodymia catalysts for diesel soot combustion, Appl. Catal. B 197 (2016) 125–137, http://dx.doi.org/10.1016/j.apcatb.2015.12.030.

[16] Q. Liang, X. Wu, X. Wu, D. Weng, Role of surface area in oxygen storage capacity of Ceria-zirconia as soot combustion catalyst, Catal. Lett. 119 (2007) 265–270, http://dx.doi.org/10.1007/s10562-007-9228-0.

[17] P. Li, W. Zhang, X. Zhang, Z. Wang, X. Wang, S. Ran, Y. Lv, Recycling, synthesis, characterization, and photocatalytic properties of flower-like Mn-doped Ceria 21 (2018) 2–7.

[18] H. Huang, J. Liu, P. Sun, S. Ye, B. Liu, Effects of Mn-doped Ceria oxygen-storage material on oxidation activity of diesel soot, RSC Adv. 7 (2017) 7406–7412, http://dx.doi.org/10.1039/C6RA27007G.

[19] O. Vasylkiv, Y. Sakka, V.V. Skorokhod, Facile synthesis of catalyticlly active CeO_2–Gd_2O_3 solid solutions for soot oxidation, J. Chem. Sci. 126 (2014) 429–435, http://dx.doi.org/10.1111/j.1551-2916.2006.00967.x.

[20] E. Aneggi, C. De Leitenburg, G. Dolcetti, A. Trovarelli, Promotional effect of rare earths and transition metals in the combustion of diesel soot over CeO_2 and CeO_2–ZrO_2, Catal. Today 114 (2006) 40–47, http://dx.doi.org/10.1016/j.cattod.2006.02.008.

[21] I. Atribak, A. Bueno-López, A. García-García, Thermally stable Ceria–Zirconia catalysts for soot oxidation by O_2, Catal. Commun. 9 (2008) 250–255, http://dx.doi.org/10.1016/j.catcom.2007.05.047.

[22] Q. Liang, A.X. Wu, A. Xiaodi, W. Ae, D. Weng, Role of surface area in oxygen storage capacity of Ceria–Zirconia as soot combustion catalyst, Catal. Lett. 119 (2007) 265–270, http://dx.doi.org/10.1007/s10562-007-9228-0.

[23] B.M. Reddy, P. Bharali, A. Gode, T. Ae, P. Saikia, A. Lakshmi, K. Ae, S.-E. Park, Catalytic efficiency of Ceria–Zirconia and Ceria–Hafnia nanocomposite oxides for soot oxidation, Catal. Lett. 123 (2008) 327–333, http://dx.doi.org/10.1007/s10562-008-9427-3.

[24] Y. Zhang, X. Zou, The catalytic activities and thermal stabilities of Li/Na/K carbonates for diesel soot oxidation, Catal. Commun. 8 (2007) 760–764, http://dx.doi.org/10.1016/j.catcom.2006.09.008.

[25] M. Fu, J. Lin, W. Zhu, J. Wu, L. Chen, B. Huang, D. Ye, Surface reactive species on MnO_x(0.4)–CeO_2 catalysts towards soot oxidation assisted with pulse dielectric barrier discharge, J. Rare Earths 32 (2014) 153–158, http://dx.doi.org/10.1016/S1002-0721(14)60045-4.

[26] K. Krishna, A. Bueno-López, M. Makkee, J.A. Moulijn, Potential rare earth modified CeO_2 catalysts for soot oxidation I. Characterisation and catalytic activity with O_2, Appl. Catal. B 75 (2007) 189–200, http://dx.doi.org/10.1016/j.apcatb.2007.04.010.

[27] S.I. Suárez-Vázquez, A. Cruz-López, C.E. Molina-Guerrero, A.I. Sánchez-Vázquez, C. Macías-Sotelo, Effect of dopant loading on the structural and catalytic properties of Mn-doped $SrTiO_3$ catalysts for catalytic soot combustion, Catalysts 8 (2018) http://dx.doi.org/10.3390/catal8020071.

[28] J.T. Kim, T.H. Lee, K.Y. Park, Y. Seo, K.B. Kim, S.J. Song, B. Park, J.Y. Park, Electrochemical properties of dual phase neodymium-doped Ceria alkali carbonate composite electrolytes in intermediate temperature, J. Power Sources 275 (2015) 563–572, http://dx.doi.org/10.1016/j.jpowsour.2014.10.139.

[29] F. Meng, N. Lin, T. Xia, J. Wang, Z. Shi, J. Lian, Q. Li, H. Zhao, F. Ma, Neodymium-doped Ceria nanomaterials: facile low-temperature synthesis and excellent electrical properties for IT-SOFCs, RSC Adv. 3 (2013) 6290, http://dx.doi.org/10.1039/c3ra22833a.

[30] M.A. Rana, M.N. Akbar, M. Anwar, K. Mustafa, S. Shakir, Z.S. Khan, Sol–Gel Fabrication of Novel Electrolytes Based on Neodymium Doped Ceria for Application in Low Temperature Solid Oxide Fuel Cells, Elsevier Ltd., 2015, http://dx.doi.org/10.1016/j.matpr.2015.11.099.

[31] M. Kamiya, E. Shimada, Y. Ikuma, M. Komatsu, H. Haneda, S. Sameshima, Y. Hirata, Oxygen self-diffusion in cerium oxide doped with Nd, J. Mater. Res. 16 (2001) 179–184, http://dx.doi.org/10.1557/JMR.2001.0029.

[32] A.M. Hernández-Giménez, L.P.D.S. Xavier, A. Bueno-López, Improving Ceria–Zirconia soot combustion catalysts by neodymium doping, Appl. Catal. A 462–463 (2013) 100–106, http://dx.doi.org/10.1016/j.apcata.2013.04.035.

[33] N.S. Priya, C. Somayaji, S. Kanagaraj, Synthesis and characterization of Nd^{3+}-doped $Ce_{0.6}Zr_{0.4}O_2$ and its doping significance on oxygen storage capacity, Rare Met. (2016) 1–6, http://dx.doi.org/10.1007/s12598-016-0698-3.

[34] J.G. Mira, V.R. Pérez, A. Bueno-López, Effect of the CeZrNd mixed oxide synthesis method in the catalytic combustion of soot, Catal. Today 253 (2015) 77–82, http://dx.doi.org/10.1016/j.cattod.2014.11.037.

[35] S.V. Chavan, P.U.M. Sastry, A.K. Tyagi, Combustion synthesis of nanocrystalline Nd-doped Ceria and Nd_2O_3 and their fractal behavior as studied by small angle X-ray scattering, J. Alloys Compd. 456 (2008) 51–56, http://dx.doi.org/10.1016/j.jallcom.2007.02.019.

[36] T. Mimani, K.C. Patil, Solution combustion of nanoscale oxides and their composites, Mater. Phys. Mech. 4 (2001) 134–137, http://dx.doi.org/10.1016/j.materresbull.2008.09.034.

[37] A. Varma, A.S. Mukasyan, A.S. Rogachev, K.V. Manukyan, Solution combustion synthesis of nanoscale materials, Chem. Rev. 116 (2016) 14493–14586, http://dx.doi.org/10.1021/acs.chemrev.6b00279.

[38] A. Varma, A.S. Mukasyan, Combustion synthesis of advanced materials: Fundamentals and applications, Korean J. Chem. Eng. 21 (2004) 527–536, http://dx.doi.org/10.1007/BF02705444.

[39] D.H. Prasad, H.Y. Jung, H.G. Jung, B.K. Kim, H.W. Lee, J.H. Lee, Single step synthesis of nano-sized NiO–$Ce_{0.75}Zr_{0.25}O_2$ composite powders by glycine nitrate process, Mater. Lett. 62 (2008) 587–590, http://dx.doi.org/10.1016/j.matlet.2007.06.006.

[40] V. Bedekar, A.K. Tyagi, Nano crystalline Ceria-neodymia solid solutions by combustion route: Effect of agglomeration on powder properties, J. Nanosci. Nanotechnol. 7 (2007) 3214–3220, http://dx.doi.org/10.1166/jnn.2007.801.

[41] A.T. Colomer, D.A. Fumo, A.R. Jurado, A.M. Segada, Nonstoichiom. La (1999) 2505–2510.

[42] V.C. Sousa, A.M. Segadaes, M.R. Morelli, R.H.G.A. Kiminami, Combustion synthesized ZnO powders for varistor ceramics, Int. J. Inorg. Mater. 1 (1999) 235–241, http://dx.doi.org/10.1016/S1466-6049(99)00036-7.

[43] S. Charojrochkul, N.L. Waraporn Nualpaeng, S. Assabumrungrat, Combustion synthesis of nanoparticles CeO_2 and $Ce_{0.9}$ $Gd_{0.1}$ $O_{1.95}$, Mater. Challenges Test. Supply Energy Resour. 1 (2012) 189–202, http://dx.doi.org/10.1007/978-3-642-23348-7.

[44] A. Mishra, R. Prasad, Effect of preparation method and calcination temperature on $LaCoO_3$ perovskite catalyst for diesel soot oxidation, Can. Chem. Trans. 3 (2015) 95–107, http://dx.doi.org/10.13179/canchemtrans.2015.03.01.0168.

[45] M. Lykaki, E. Pachatouridou, E. Iliopoulou, S.A.C. Carabineiro, M. Konsolakis, Impact of the synthesis parameters on the solid state properties and the CO oxidation performance of Ceria nanoparticles, RSC Adv. 7 (2017) 6160–6169, http://dx.doi.org/10.1039/C6RA26712B.

[46] D. Hari Prasad, H.R. Kim, J.W. Son, B.K. Kim, H.W. Lee, J.H. Lee, Superior compositional homogeneity and long-term catalytic stability of Ni-$Ce_{0.75}Zr_{0.25}O_2$ cermets prepared via glycine nitrate process, Catal. Commun. 10 (2009) 1334–1338, http://dx.doi.org/10.1016/j.catcom.2009.02.017.

[47] N. Kikukawa, M. Takemori, Y. Nagano, M. Sugasawa, S. Kobayashi, Synthesis and magnetic properties of nanostructured spinel ferrites using a glycine-nitrate process, J. Magn. Magn. Mater. 284 (2004) 206–214, http://dx.doi.org/10.1016/j.jmmm.2004.06.039.

[48] Y.P. Fu, S.H. Chen, Preparation and characterization of neodymium-doped Ceria electrolyte materials for solid oxide fuel cells, Ceram. Int. 36 (2010) 483–490, http://dx.doi.org/10.1016/j.ceramint.2009.09.013.

[49] J. Zhang, C. Ke, H. Wu, J. Yu, J. Wang, Lattice thermal expansion and solubility limits of neodymium-doped Ceria, J. Solid State Chem. 243 (2016) 57–61, http://dx.doi.org/10.1016/j.jssc.2016.08.009.

[50] T. Vinodkumar, B.M. Reddy, Tuning the Structural and Catalytic Properties of Ceria By Doping with Zr^{4+}, La^{3+} and Eu^{3+} Cations, 2015, http://dx.doi.org/10.1007/s12039-015-0891-1.

[51] B. Choudhury, A. Choudhury, Lattice distortion and corresponding changes in optical properties of CeO_2 nanoparticles on Nd doping, Curr. Appl. Phys. 13 (2013) 217–223, http://dx.doi.org/10.1016/j.cap.2012.07.014.

[52] R. Yuvakkumar, S.I. Hong, Nd2O3: novel synthesis and characterization, J. Sol-Gel Sci. Technol. 73 (2014) 511–517, http://dx.doi.org/10.1007/s10971-015-3629-0.

[53] I. Shajahan, J. Ahn, P. Nair, S. Medisetti, S. Patil, V. Niveditha, G. Uday Bhaskar Babu, H.P. Dasari, J.H. Lee, Praseodymium doped Ceria as electrolyte material for IT-SOFC applications, Mater. Chem. Phys. 216 (2018) 136–142, http://dx.doi.org/10.1016/j.matchemphys.2018.05.078.

[54] H. Gu, M.D. Soucek, Preparation and characterization of monodisperse cerium oxide nanoparticles in hydrocarbon solvents, Chem. Mater. 19 (2007) 1103–1110, http://dx.doi.org/10.1021/cm061332r.

[55] S. Mochizuki, F. Fujishiro, The photoluminescence properties and reversible photoinduced spectral change of CeO_2 bulk, film and nanocrystals, Phys. Status Solidi Basic Res. 246 (2009) 2320–2328, http://dx.doi.org/10.1002/pssb.200844419.

[56] S. Pengpanich, V. Meeyoo, T. Rirksomboon, Oxidation of methane over Nb-doped $Ce_{0.75}Zr_{0.25}O_2$ mixed oxide solid solution catalysts, J. Chem. Eng. Japan. 38 (2005) 49–53, http://dx.doi.org/10.1252/jcej.38.49.

[57] A. Getsoian, Z. Zhai, A.T. Bell, Band-gap energy as a descriptor of catalytic activity for propene oxidation over mixed metal oxide catalysts, J. Am. Chem. Soc. 136 (2014) 13684–13697, http://dx.doi.org/10.1021/ja5051555.

[58] D.H. Prasad, S.Y. Park, H.I. Ji, H.R. Kim, J.W. Son, B.K. Kim, H.W. Lee, J.H. Lee, Structural characterization and catalytic activity of $Ce_{0.65}Zr_{0.25}RE_{0.1}O_{2-\delta}$ nanocrystalline powders synthesized by the glycine-nitrate process, J. Phys. Chem. C 116 (2012) 3467–3476.

[59] J.P. Holgado, R. Alvarez, G. Munuera, Study of CeO_2 XPS spectra by factor analysis: Reduction of CeO_2, Appl. Surf. Sci. 161 (2000) 301–315, http://dx.doi.org/10.1016/S0169-4332(99)00577-2.

[60] P. Dutta, S. Pal, M.S. Seehra, Y. Shi, E.M. Eyring, R.D. Ernst, Concentration of Ce 3+ and oxygen vacancies in cerium oxide nanoparticles, Chem. Mater. 18 (2006) 5144–5146, http://dx.doi.org/10.1021/cm061580n.

[61] Y. Wei, J. Liu, Z. Zhao, A. Duan, G. Jiang, C. Xu, J. Gao, H. He, X. Wang, Three-dimensionally ordered macroporous $Ce_{0.8}Zr_{0.2}O_2$-supported gold nanoparticles: Synthesis with controllable size and super-catalytic performance for soot oxidation, Energy Environ. Sci. 4 (2011) 2959–2970, http://dx.doi.org/10.1039/c0ee00813c.